Properties of the 3D photonic nanojet based on the refractive index of surroundings

Hongxing Ding (丁红星)[1,2*], Lili Dai (戴丽莉)[1], and Changchun Yan (闫长春)[3]

[1]*Department of Physics, Lianyungang Teachers College, Lianyungang 222006, China*

[2]*Department of Applied Physics, Nanjing University of Science and Technology, Nanjing 210094, China*

[3]*School of Physics and Electronic Engineering, Xuzhou Normal University, Xuzhou 221116, China*

[*]*E-mail: dinghxing@126.com*

Received Match 1, 2010

We exhibit a three-dimensional (3D) photonic nanojet based on a dielectric microsphere irradiated by a plane wave with the finite-difference time-domain (FDTD) method. We investigate the influence of the refractive index of the surrounding on the properties of the nanojet by simulating the electric field distributions in it. The simulation results show that, by optimally choosing the size of the sphere and the ratio of the refractive indices of the sphere and the surrounding, the focus point can occur just on the surface of the sphere even if the refractive index of the surrounding is changed. Additionally, the peak amplitude of the nanojet increases with increasing the refractive index of the surrounding. However, the decay length and the jet width of the nanojet decrease simultaneously. These effects may have potential applications in observation or manipulation of nano-objects such as antibodies in biology. In nanojet-enabled optical data storage, the photonic nanojet may be also helpful for improving data-storage capacities and retrieval speed by controlling the field amplitude, the decay length, and jet width of the nanojet.

OCIS codes: 180.0180, 290.4020.

doi: 10.3788/COL20100807.0706.

The photonic nanojet[1−13], which was reported and named by Chen *et al.* for the first time in 2004[1], is a high-intensity and sub-diffraction beam emerging from the back surface of a lossless dielectric microcylinder or microsphere illuminated by a plane wave. If the ratio of its refractive index to the refractive index of the background medium is less than about 2[2], this beam will still appear even though the diameter of the cylinder or sphere varies in a wide range. Depending on the refractive index, the focus point (defined here as the point with a maximum intensity at the optical axis) can be inside or outside the microlens[3]. The nanojet propagates into the surrounding medium with divergence reaching several wavelengths (λ) while it maintains a narrow transverse beam width smaller than λ. Another remarkable property of the nanojet is that it can significantly enhance the backscattering of visible light by nanometer-scale particles located within the jet, which has been demonstrated by numerical studies[4−6]. This could yield a potential novel ultramicroscopy technique using visible light to detect proteins, viral particles, and even single molecules, and to monitor molecular synthesis and aggregation processes in many areas of biology, chemistry, material sciences, and tissue engineering.

These studies all assumed that the refractive index of the surrounding is 1 so as to get a higher ratio of the refractive indices of the sphere and the surrounding. The benefit of doing so is of advantage to numerical calculation. In practice, however, the materials surrounding the nanojet are changed, which results in relatively high requirements in designing the nanojet. In this letter, we study the influence of the refractive index of the surrounding on the properties of the photonic jet formed by a dielectric microsphere based on the assumption that the refractive index of the dielectric microsphere or the ratio of the refractive index of the sphere and the surrounding are unchanged. The exhibited characteristics are conducive to controlling the nanojet in practical applications.

We suppose four tunable parameters here. They are the refractive index of the particle n_1, the refractive index of the surrounding n_2, the wavelength of the incident plane wave λ, and the radius of the particle R, respectively. In order to characterize the nanojets, additional four parameters are also introduced (see Fig. 1(a)). The first one is peak amplitude, unit amplitude for an incident plane wave, which is the maximum amplitude of the field in the nanojet. The second one is radial shift, which denotes the radial distance of the point of peak amplitude away from the surface of the particle. The third one is decay length, which is the radial distance between the point of peak amplitude and the point at which the field decays to 1/e of the peak amplitude. The last one is jet width, which is twice the distance of the point of peak amplitude away from the points where the field decays to 1/e of the peak value in the tangential direction[5].

We assume that a dielectric sphere is illuminated by a Y-polarized and Z-propagating plane wave with unit intensity and wavelength λ=400 nm. The geometry is shown in Fig. 1(b). The sphere is set in a wafer with 4.00-μm width (X), 4.00-μm depth (Y), and 6.00-μm length (Z). The time step is chosen as Δt=3.34×10^{-17} s. The resulting mesh grid is (0.02 (ΔX)× 0.02 (ΔY)× 0.02 (ΔZ)) μm. Using the commercial software OptiFDTD finite-difference time-domain (FDTD) a software, we simulated the field distribution in the photonic nanojet for R=2 μm, n_1=2.385, and n_2=1.6. The corresponding results are shown in Fig. 2.

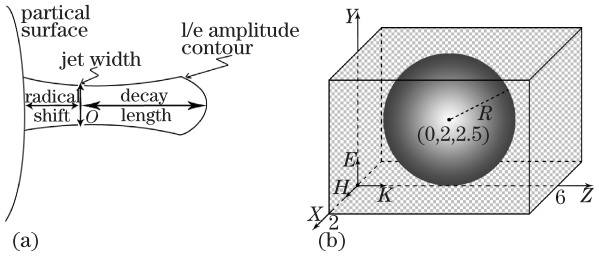

Fig. 1. (a) Properties of a nanojet. The peak amplitude is at point O. (b) Schematic of the nanojet-genarated structure with the coordinate system. The unit is μm.

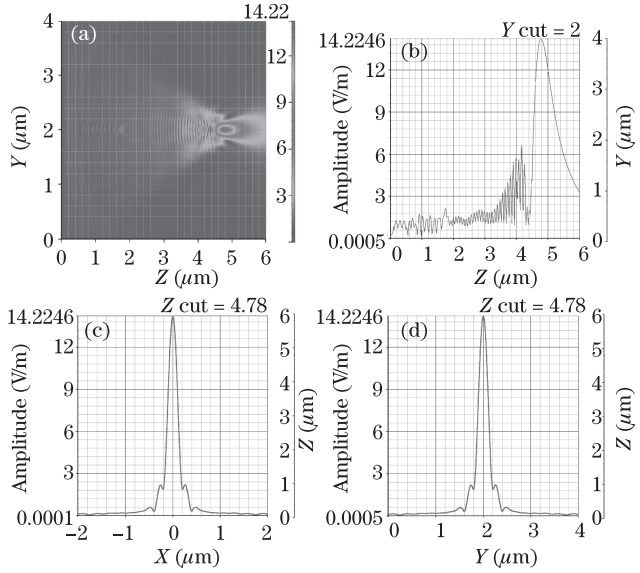

Fig. 2. Normalized electric field intensity relative to the incident illumination for the isolated 2-μm diameter microsphere at λ=400 nm. The cubic grid-cell size is 20 nm. (a) The photonic nanojet observed in the Y-Z longitudinal cut-plane (X=0); (b) the cutting plane (X=0,Y=2); (c) the cutting plane (X=0, Z=4.78); (d) the cutting plane (Y=2, Z=4.78).

Figure 2(a) depicts the electric field distribution in the Y-Z plane with X=0. Evidently, the electric-field peak emerges from the shadow-side surface of the microsphere and propagates with little divergence into the surrounding medium. There-dimensional (3D) data can also be represented in a two-dimensional (2D) graph when one dimension is fixed. Figure 2(b) is the cutting plane (X=0, Y=2), while Figs. 2(c) and (d) are the cutting plane (X=0, Z=4.78) and (Y=2, Z=4.78), respectively. The slider to the right of the graph represents the cutting axis. The knob on the slider shows the current cutting value. When the knob is moved, the cutting value changes. According to the definitions of the radial shift and the decay length, Fig. 2(b) shows that the decay length and radial shift of the nanojet are about 820 nm (more than 2λ) and 280 nm, respectively, and the peak amplitude is 14.2246 V/m. Analyzing the data in Figs. 2(c) and (d), we can obtain that the jet widths are equal to 260 and 280 nm, respectively. The width is smaller than that of the incident wavelength, indicating that the diffraction limit is broken. This may provide a new ultramicroscopy technique for using visible light to detect and image nanoparticles. Some studies[14−16] have been done about the applications of sub-diffraction. Moreover, due to the polarization of the incident wave, the photonic nanojet does not have a cylindrical symmetry. We also study the influence of the refractive index of the surrounding on the properties of the photonic nanojet when the refractive index of the dielectric microsphere is unchanged. Figures 3(a), (b), and (c) show the steady-state electric fields for n_2=1.2, 1.6, and 1.8, respectively. With the increase of n_2, it is evident that the electric-field peak shifts from the inside to the outside of the microsphere along the propagating direction. The peak amplitudes are 14.9, 14.2246, and 12.53 V/m, respectively. The Z-axis coordinate values for these peaks are 3.9, 4.78, and 5.36 μm, respectively. Therefore, by optimally choosing the refractive index of the surrounding, the focus point can occur just on the surface of the sphere with Z=4.5 μm.

The radial shift is plotted as a function of R (radius of the microsphere) in Fig. 4 for η=1.49 and n_1=2.385, where η is the ratio of the refractive indices of the sphere and the surrounding. Obviously, the radial shift decreases with the reduction of R, and the peak amplitude goes back into the sphere when R=0.6 μm. Therefore, by optimally choosing R, the radial shift may become zero. Our further studies show that the value of η, satisfying condition that the radial shift is zero, is a function of R. And η also increases with R. Otherwise, when $R < \lambda$, the photonic nanojet cannot be generated because, in the Rayleigh case, the maximum intensity is not on the optical axis in the near field.

Below, we will investigate characteristics of the photonic nanojet when η=n_1/n_2 is unchanged. We assume η=1.59. Figure 5(a) shows the field amplitude along the vertical axis at the center of the jet as a function of the refractive index of the surrounding and the distance in

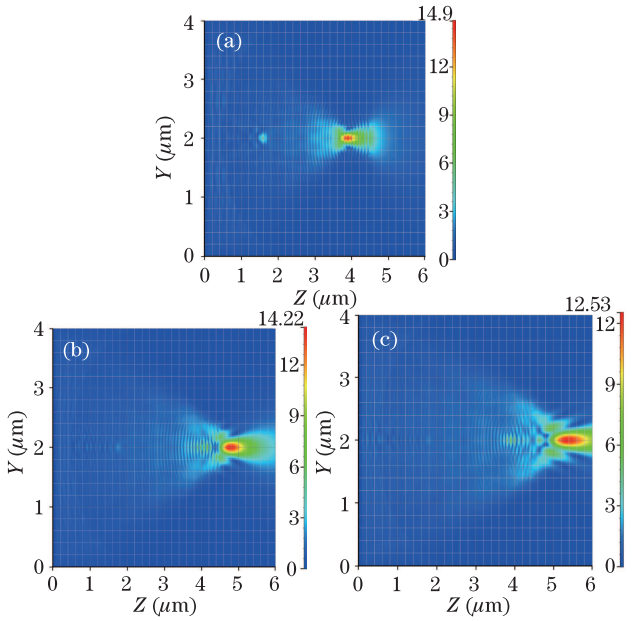

Fig. 3. Electric field distributions of a photonic nanojet with the increasing refractive index of the surrounding mediumn_2. The radius of the microsphere is R=2 μm, and its refractive index is n_1=2.385. This microsphere is illuminated by a plane wave with the wavelength of λ=400 nm in medium 2, and it is embedded in an infinite medium. (a) n_2 = 1.2; (b) n_2 =1.6; (c) n_2 = 1.8.

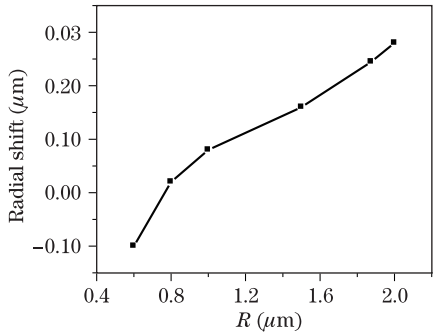

Fig. 4. Radial shift as a function of R when η=1.49 and n_1=2.385.

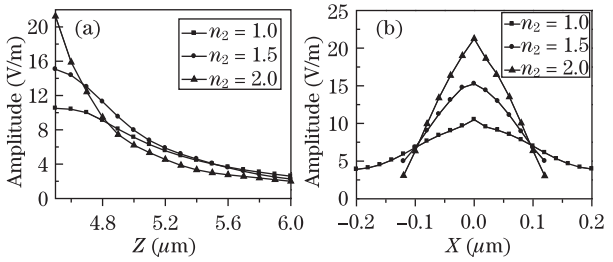

Fig. 5. Field amplitudes for η=1.59 with n_2=1.0, 1.5, and 2.0, respectively. R and λ are the same as those in Fig. 3. (a) Peak amplitude as a function of the distance in the Z direction (X=0, Y=2); (b) peak amplitude as a function of the distance in the X direction (Y=2, Z=4.5).

the Z direction. From this figure, we can see that the peak amplitudes corresponding to different refractive indices (n_2=1.0, 1.5, and 2.0) occur just on the surface of the sphere (Z=4.5 μm). Their values are 10.49, 15.03, and 21.36 V/m, respectinely. It can be also seen that the decay length of the nanojet decreases from 1040 to 380 nm with the increasing refractive index of the surrounding from 1.0 to 2.0. Figure 5(b) shows the field amplitude along the horizontal axis at the best focus point of the jet (Z=4.5 μm) as a function of the refractive index of the surrounding and the distance in the X direction. The jet widths corresponding to n_2=1.0, 1.5, 2.0 are 400, 260, and 180 nm, respectively. It indicates that the peak amplitude of the nanojet monotonically increases with the growth of the refractive index of surrounding. Unfortunately, the decay length and jet width of the nanojet decrease simultaneously.

In conclusion, we have simulated the electric field distributions in the 3D photonic nanojet based on a dielectric microsphere illunrinated by a plane wave with the FDTD method. The simulation results show that a sub-diffraction non-evanescent focus beam is generated at the shadow side of the dielectric microsphere. By optimally choosing the size and the ratio of the refractive indices of the sphere and the surrounding, the focus point can occur just on the surface of the sphere even if the refractive index of the surrounding is changed. Additionally, the peak amplitude of the nanojet increases with the increasing refractive index of the surrounding. However, the decay length and the jet width of the nanojet decrease simultaneously. These effects may have potential applications in observation or manipulation of nano-objects such as antibodies in biology. In nanojet-enabled optical data storage[17], the photonic nanojet may also be helpful for improving data-storage capacities and retrieval speed by controlling the field amplitude, the decay length, and the jet width of the nanojet.

References

1. Z. Chen, A. Taflove, and V. Backman, Opt. Express **12,** 1214 (2004).
2. S.-C. Kong, A. V. Sahakian, A. Heifetz, A. Taflove, and V. Backman, Appl. Phys. Lett. **92,** 211102 (2008).
3. S. Lecler, Y. Takakura, and P. Meyrueis, Opt. Lett. **30,** 2641 (2005).
4. X. Li, Z. Chen, A. Taflove, and V. Backman, Opt. Express **13,** 526 (2005).
5. Z. Chen, A. Taflove, X. Li, and V. Backman, Opt. Lett. **31,** 196 (2006).
6. A. Heifetz, K. Huang, A. V. Sahakian, X. Li, A. Taflove, and V. Backman, Appl. Phys. Lett. **89,** 221118 (2006).
7. A. V. Itagi and W. A. Challener, J. Opt. Soc. Am. A **22,** 2847 (2005).
8. S. Lecler, S. Haacke, N. Lecong, O. Crégut, J.-L. Rehspringer, and C. Hirlimann, Opt. Express **15,** 4935 (2007).
9. W. Wu, A. Katsnelson, O. G. Memis, and H. Mohseni, Nanotechnology **18,** 485302 (2007).
10. A. Heifetz, J. J. Simpson, S.-C. Kong, A. Taflove, and V. Backman, Opt. Express **15,** 17334 (2007).
11. M. Gerlach, Y. P. Rakovich, and J. F. Donegan, Opt. Express **15,** 17343 (2007).
12. P. Ferrand, J. Wenger, A. Devilez, M. Pianta, B. Stout, N. Bonod, E. Popov, and H. Rigneault, Opt. Express **16,** 6930 (2008).
13. A. M. Kapitonov and V. N. Astratov, Opt. Lett. **32,** 409 (2007).
14. Z. Mao, C. Wang, and Y. Cheng, Chinese J. Laser (in Chinese) **35,** 1283 (2008).
15. C. Guo, W. Ye, X. Yuan, J. Zhang, C. Zeng, and J. Ji, Acta Opt. Sin. (in Chinese) **29,** 3272 (2009).
16. Y. Chen, D. Zhao, J. Zhang, J. Zhu, and X. Wang, Acta Opt. Sin. (in Chinese) **28,** 1031 (2008).
17. S.-C. Kong, A. Sahakian, A. Taflove, and V. Backman, Opt. Express **16,** 13713 (2008).